**Eksakta** : Berkala Ilmiah Bidang MIPA
VOLUME 27 NO 05 2026, pp 912-931
ISSN : Print 1411-3724 — Online 2549-7464
DOI : https://doi.org/10.24036/eksakta/vol27-iss05/756

Eksakta
Berkala Ilmiah Bidang MIPA
http://www.eksakta.ppj.unp.ac.id/index.php/eksakta

*Article*

# Intelligent IoT-based Solar Tracker Using Fuzzy Logic Takagi-Sugeno Kang for Energy Optimization for Melon Hydroponic Monitoring

**Muhammad Ghifari Fadza Thoriq[1], Nurhayati Nurhayati[1*], Ruqayyah Hassan Labo[2], Raimundo Eider Figueredo[3], Nurulazlina Ramli[4]**

[1]Department of Electrical Engineering, Faculty of Engineering, Universitas Negeri Surabaya, Surabaya, Indonesia
[2]Department of Electronics and Telecommunications Engineering, Faculty of Engineering, Ahmadu Bello University, Zaria, Nigeria
[3]Maxwell Microwave and Applied Electromagnetism Laboratory, Instituto Federal de São Paulo (IFSP), Cubatão, Brazil
[4]Centre for Advanced Electrical & Electronic System (CAEES), SEGi University Petaling Jaya, Selangor, Malaysia

**Article Info**

***Article history*** *:*
Received September 03, 2026
Revised October 07, 2026
Accepted October 12, 2026
Published October 30, 2026

***Keywords*** *:*
Fuzzy logic,
takagi sugeno kang,
melon hydroponics,
solar tracker,
energy optimization

**Abstract.** Hydroponic melon quality depends on tightly controlled pH, TDS, and water level, requiring round-the-clock monitoring and uninterrupted off-grid power, yet fixed-tilt panels lose energy as the sun moves. This study develops a single-axis solar tracker using a Zero-Order Takagi-Sugeno-Kang (TSK) fuzzy controller, whose rules output constant servo angles combined by a weighted average, avoiding Mamdani-style centroid defuzzification and suiting an ESP32-S3 that also runs the monitoring node. Two LDR sensors feed five triangular membership functions to set five servo positions, with a deadband suppressing unnecessary movement. Five-day field trials in Jombang, Indonesia, using INA219 modules gave mean daily yield of 243.78 Wh versus 193.23Wh for a fixed panel (+25.91%), with the servo held stationary 55.3% of the time. Harvest exceeded the node's estimated 115.88 Wh/day load on all five days (2.1× on average; fixed panel 1.7×), supporting energy-autonomous 24/7 operation of the IoT melon hydroponic monitoring system.

*This is an open acces article under the CC-BY license.*

This is an open access article distributed under the Creative Commons 4.0 Attribution License, which permits unrestricted use, distribution, and reproduction in any medium, provided the original work is properly cited. ©2026 by author.

***Corresponding Author :***
Nurhayati Nurhayati
Department of Electrical Engineering, Faculty of Engineering, Universitas Negeri Surabaya, Surabaya, Indonesia
Email : nurhayati@unesa.ac.id

## 1. Introduction

Photovoltaic (PV) systems support off-grid distributed energy [1-2]. Solar tracking improves energy capture in equatorial East Java, where mean daily irradiance is approximately 4.8 kWh/m²/day [3-4]. Fixed-tilt panels lose yield as solar azimuth and elevation change [5], threatening continuous operation of self-powered remote greenhouse monitoring [6-7]. Single-axis tracking typically increases daily yield by 20–40% [8-10]. Light Dependent Resistors (LDRs) provide inexpensive closed-loop feedback through a differential irradiance signal related to angular misalignment [11-12]. However, ON/OFF and fixed-threshold controllers lack proportional error reasoning and can cause servo hunting and mechanical wear under fluctuating tropical irradiance [13].

The always-on Internet of Things (IoT) platform uses an ESP32-S3 to sample analog pH, total dissolved solids (TDS)/electrical conductivity, and HC-SR04 water-level sensors and return readings through a Wi-Fi Telegram bot [14]. Comparable agricultural ESP32 nodes consume 6–9 Wh/day with active sampling, deep sleep, and intermittent transmission [15-16]. Continuously excited pH/TDS probes and repeated HC-SR04 pulses add to that baseline [17]. Harvest must cover sensing and telemetry before supporting multi-day cloudy-weather autonomy [18]. Avoiding a daily battery energy deficit therefore links tracking performance directly to continuous melon hydroponic monitoring.

Fuzzy control maps uncertain sensor errors to smooth nonlinear actuator commands without an explicit plant model [19]. Classical Proportional-Integral-Derivative (PID) control requires accurate modeling and gain tuning as cloud cover, humidity, and seasonal solar paths change [20]. Mamdani control avoids this modeling burden but requires centroid integration whose cost scales with output resolution [21]. Zero-Order Takagi-Sugeno-Kang (TSK) instead combines constant singleton consequents by weighted average, providing model-free, deterministic inference suited to a battery-powered microcontroller [22].

Embedded intelligent tracking is replacing open-loop and threshold control [23-24], but controller-cost measurements on hardware sharing an IoT payload remain scarce. Reported ESP32 Zero-Order TSK-type inference takes under 2.5 ms and less than 30 KB RAM [25]. A pointer-array microcontroller fuzzy implementation achieved 20 ms closed-loop settling with low overhead [26]. Eliminating centroid integration reduces CPU cycles, firmware latency, and active-mode duty cycle [27], fitting the ESP32-S3's dual-core 240 MHz processor, 12-bit ADC, and energy constraints.

Five integration gaps remain. Conventional LDR trackers lack intelligent reasoning [28-29]. Mamdani trackers lack deadband filtering and quantitative energy monitoring [30-31]. GPS/astronomical hybrids add complexity without IoT energy quantification [32]. Agricultural trackers generally lack real-time INA219 current-voltage monitoring [33]. And IoT hydroponic nodes use fixed panels without intelligent harvesting optimization [34-35]. The proposed field-validated platform addresses these gaps together.

To the authors' knowledge, the combination is novel in three respects. Unlike earlier Mamdani LDR trackers [36], singleton Zero-Order TSK inference removes centroid integration and provides deterministic ESP32-S3 execution [37]. Deadband filtering and five-position quantization, previously reported separately [38-39], jointly reduce unnecessary actuation while preserving coverage and supporting actuator life in humid greenhouses. Dual INA219 modules additionally provide a hardware-verified tracker-versus-fixed energy comparison, advancing beyond theoretical or simulated estimates on a self-powered melon hydroponic platform. Field validation examines

energy yield across clear, partly cloudy, and overcast conditions, actuator stability, and the ability of harvested energy to sustain sensing and telemetry through the day-night cycle.

The study contributes an ESP32-S3 implementation of a single-input Zero-Order TSK tracker with five triangular sets and discrete servo positions. It combines deadband filtering with quantization and dual INA219 panel/battery monitoring for a hardware energy comparison. Field validation in tropical equatorial Banjarsari Village, Jombang, East Java, Indonesia, includes Telegram energy and water-quality telemetry.

## 2. Methods

### 2.1 System Architecture and Research Focus

The platform integrates Zero-Order TSK tracking with IoT monitoring [6], [40], focusing on photovoltaic optimization [1-3]. A servo orients the 100 Wp monocrystalline panel. A Solar Charge Controller (SCC) charges the 12 V/45 Ah battery, and a buck converter supplies the ESP32-S3 at 5 V [7], [17] (Figure 1).

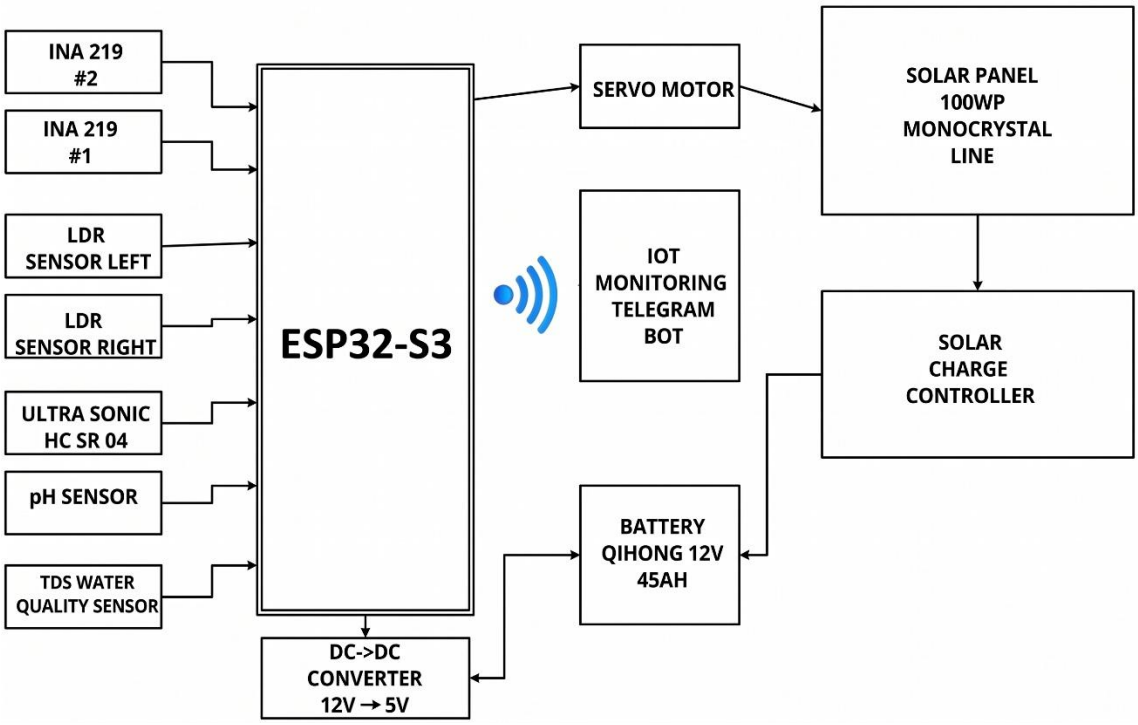



**Figure 1.** Overall Design Block Diagram of System

### 2.2 Research Location and Site Characterization

Trials used a hydroponic greenhouse in Banjarsari Village, Jombang, East Java, Indonesia (7°33'36.64"S, 112°09'09.24"E, Figure 2). Mean daily irradiance during testing was approximately 4.5–5.2 kWh/m²/day. Intermittent tropical cloud cover challenged adaptive tracking under equatorial conditions comparable to Ismail et al. [33].




**Figure 2.** Google Maps View of the Experiment Location in Banjarsari Village, Jombang.

### 2.3 Hardware Configuration

Table 1 lists the hardware. The ESP32-S3 offers 12-bit ADC (0–4095), Wi-Fi, and dual-core 240 MHz processing. Upper-corner GL5528 LDRs face outward/upward toward separate sky hemispheres, generating differential feedback without a shadow-casting baffle [13], as in comparable trackers [29].

**Table 1.** Hardware Configuration.

| No | Component | Specification / Function |
|---|---|---|
| 1 | ESP32-S3 | Xtensa LX7 240 MHz, Wi-Fi + BT, ADC 12-bit |
| 2 | Solar Panel | 100 Wp Monocrystalline PV |
| 3 | SCC | PWM Solar Charge Controller 12 V/30 A |
| 4 | Battery | Qihong Li-ion 12 V/45 Ah |
| 5 | Buck Converter | DC-DC Step-Down 12 V → 5 V/3 A |
| 6 | Servo Motor | TD8120MG, 180° range, 20 kg·cm |
| 7 | LDR Sensor (×2) | GL5528, voltage-divider config., ADC 12-bit |
| 8 | INA219 No. 1 | I²C, 0x40, panel → SCC (power monitoring) |
| 9 | INA219 No. 2 | I²C, 0x41, battery → load (battery monitoring) |
| 10 | pH Sensor | pH 4502C Analog, BNC probe, pH 0–14 |
| 11 | TDS Sensor | Analog TDS PPM, 0–2000 ppm |
| 12 | RTC DS3231 | I²C Real-Time Clock |
| 13 | HC-SR04 | Ultrasonic, 2 cm–400 cm range, water-level monitoring |

The 180° TD8120MG has approximately 20 kg·cm stall torque (vendor range 15–22.8 kg·cm at 4.8–7.4 V), comparable to other LDR trackers [12], [28]. INA219s (I²C, 0.1 Ω shunt, ±1% accuracy) measure panel/battery voltage-current for energy quantification (Section 2.4.10) [7]. Figure 3 connects the ESP32-S3, LDRs, servo, INA219s, pH/TDS probes, and HC-SR04. The 100 Wp panel supplies the SCC/battery. INA219s monitor energy parameters. Integrated Wi-Fi returns combined nutrient-solution and tracker readings through Telegram on request.

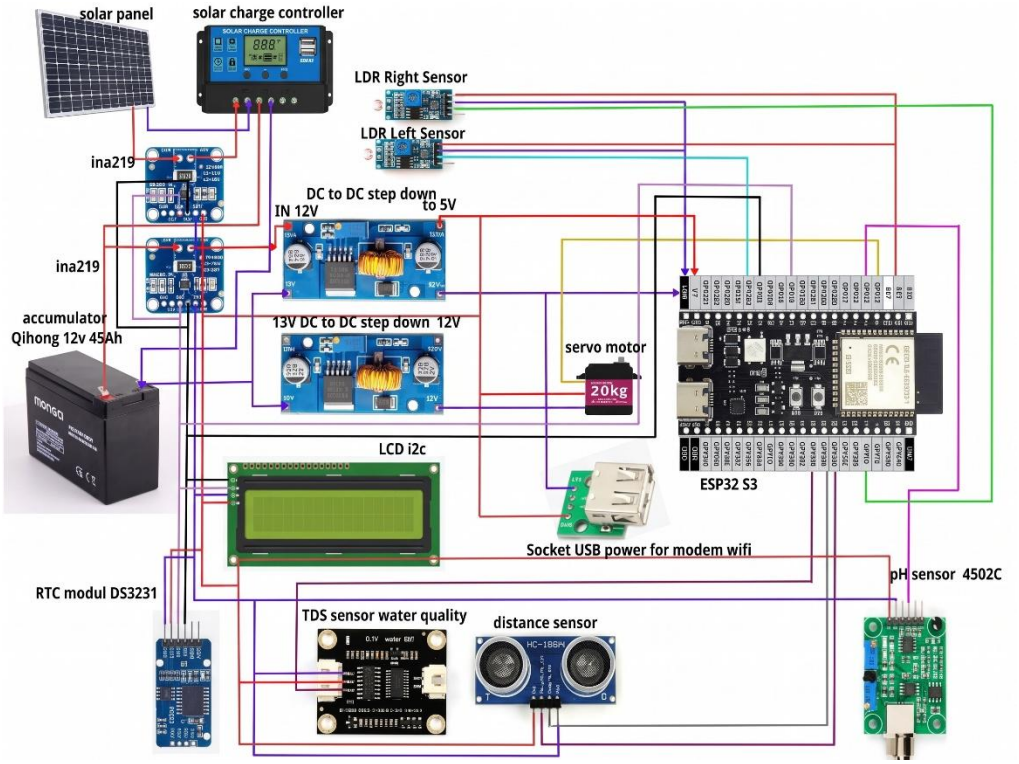



**Figure 3.** Complete Wiring Diagram of the Proposed System.

The lower battery compartment improves stability by reducing the center of gravity. Four casters permit relocation. Figure 4 shows the integrated tracking, harvesting, hydroponic sensing, and Telegram platform.

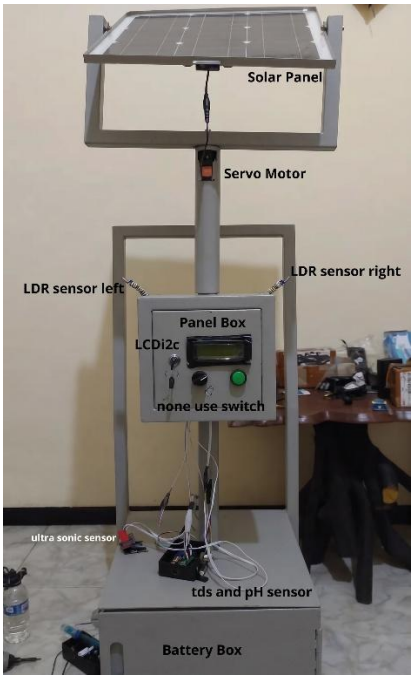



**Figure 4.** Physical Prototype of the IoT-based Hydroponic Monitoring and Zero-Order Fuzzy TSK Solar Tracking System.

### 2.4 Zero-Order Fuzzy TSK Solar Tracker Design

The complete Fuzzy TSK firmware pipeline is described below, directly consistent with the firmware implementation on the ESP32-S3.

#### 2.4.1 Input Variable

The fuzzy input e is the dual-LDR ADC differential in Equation (1) [11], [31].

$$e = LDR_{Left} - LDR_{Right}, e \in [-4095,4095] \quad (1)$$

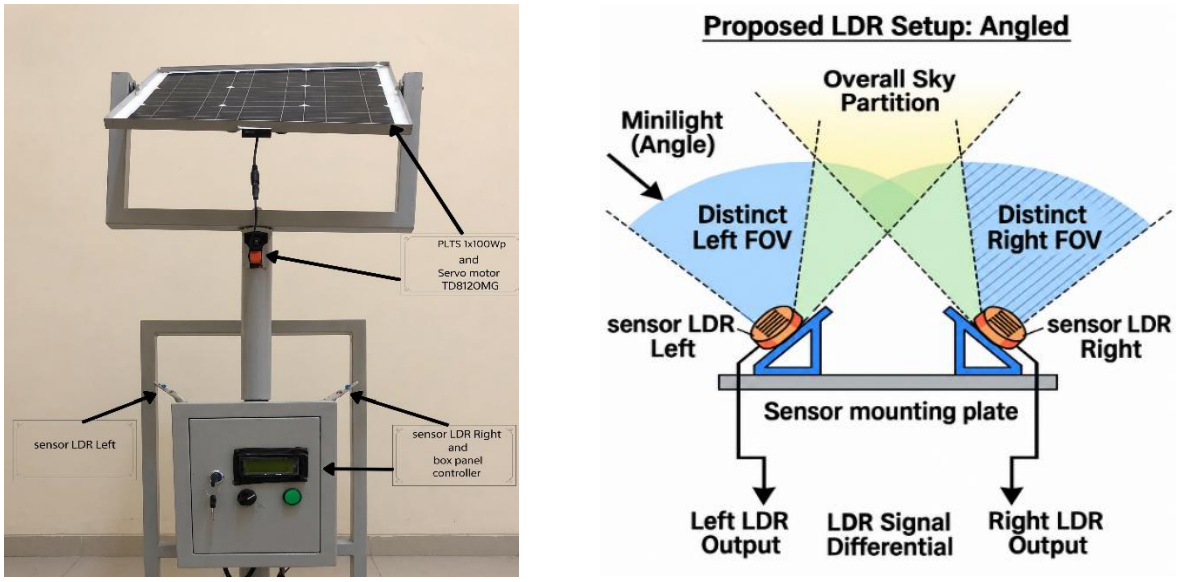
LDR_Left and LDR_Right are 12-bit voltage-divider readings in [0, 4095]. Positive e indicates greater left irradiance, with the sun left of the panel's facing direction [28], [29].

#### 2.4.2 Deadband Suppression and LDR Physical Configuration

Before inference, Equation (2) suppresses small-error servo hunting identified by Thungsuk et al. [8] and Sanyal et al. [30], reducing noise-driven actuator wear [38-39].

$$if\ |e| < LDR_{deadband} \rightarrow maintain\ current\ servo\ position \quad (2)$$

where $LDR_{deadband}$ = 300 ADC counts, equivalent to approximately 7.32% of the full 0–4095 12-bit range.




(a) (b)

**Figure 5.** The proposed dual LDR tracking configuration without a physical shadow-casting barrier. (a) Physical mounting of the dual GL5528 LDR sensors on the field prototype. (b) Schematic diagram illustrating the angled mounting setup that creates an optical overall sky partition and distinct left-right fields of view.

Top-corner GL5528 brackets face outward/upward into separate sky hemispheres, generating differential error *e* without a divider (Figure 5) [13], as in comparable trackers [29]. The serviceable assembly exposes one stainless steel part to humidity/UV. Equation (2)'s deadband compensates for the softer optical transition near e ≈ 0 relative to a divider, suppressing hunting.

### 2.4.3 Triangular Membership Function

Equation (3) defines the triangular membership function (trimf) used by all five sets for computationally efficient embedded inference [23], [27], [41].

$$\mu(x) = 0 \text{ if } x \le a \text{ or } x \ge c;\ (x-a)/(b-a) \text{ if } a < x < b;\ (c-x)/(c-b) \text{ if } b \le x < c \quad (3)$$

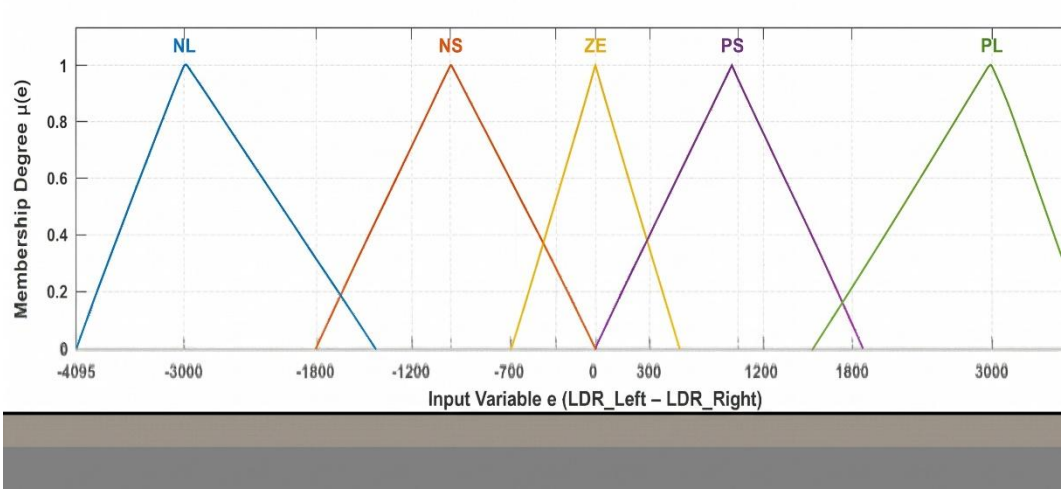



**Figure 6.** Triangular Membership Functions of the Five Fuzzy Sets over Input Domain $e \in [-4095, 4095]$.

ZE holds near-aligned positions despite noise/irradiance fluctuations. NL, NS, PS, and PL determine realignment direction and magnitude.

### 2.4.4 Five Fuzzy Sets

Table 2 specifies the NL, NS, ZE, PS, and PL triangles over $e \in [-4095, 4095]$. They cover the differential range proportionally [23], [30], with near-alignment sensitivity in ZE ($|e| < 300$ ADC counts) [31].

**Table 2.** Triangular Membership Function Parameters

| Fuzzy Set | Linguistic Meaning | a (left) | b (peak) | c (right) |
|---|---|---|---|---|
| NL (Negative Large) | Sun far to the right | −4095 | −3000 | −1200 |
| NS (Negative Small) | Sun slightly to the right | −1800 | −700 | 0 |
| ZE (Zero) | Panel aligned | −300 | 0 | 300 |
| PS (Positive Small) | Sun slightly to the left | 0 | 700 | 1800 |
| PL (Positive Large) | Sun far to the left | 1200 | 3000 | 4095 |

### 2.4.5 Five-Rule Base and Zero-Order Singleton Consequents

Each Zero-Order TSK set has one IF-THEN rule with a constant singleton consequent [27]. Unlike linear first-order TSK [41] or Mamdani output fuzzy sets [22], this permits analytical defuzzification without centroid integration (Table 3).

**Table 3.** Five-Rule Zero-Order TSK Rule Base

| Rule | IF e IS | Fuzzy Set | THEN servo = | Interpretation |
|---|---|---|---|---|
| R1 | e IS NL | Negative Large | z1 = 0° | Panel rotates fully right (sun far right) |
| R2 | e IS NS | Negative Small | z2 = 45° | Panel rotates slightly right |
| R3 | e IS ZE | Zero | z3 = 90° | Panel stays centered (aligned) |
| R4 | e IS PS | Positive Small | z4 = 135° | Panel rotates slightly left |
| R5 | e IS PL | Positive Large | z5 = 180° | Panel rotates fully left (sun far left) |

### 2.4.6 Defuzzification Weighted Average

Equation (4) gives the analytical Zero-Order TSK weighted average [27]. First-order T–S instead uses input-dependent linear consequents [41].

$$\theta^* = \frac{\Sigma(\mu i \times zi)}{\Sigma \mu i, i=1..5[default: 90° \; if \; \Sigma \mu i = 0]} \quad (4)$$

### 2.4.7 Servo Quantization

Table 4 quantizes θ* to five positions, following Thungsuk et al. [8], suppressing oscillation while retaining solar-angle coverage.

**Table 4.** Servo Quantization Boundaries

| Defuzzified θ* Range | Quantized Servo Position |
|---|---|
| 0° ≤ θ* < 22.5° | 0° |
| 22.5° ≤ θ* < 67.5° | 45° |
| 67.5° ≤ θ* < 112.5° | 90° |
| 112.5° ≤ θ* < 157.5° | 135° |
| 157.5° ≤ θ* ≤ 180° | 180° |

Quantization limits power-consuming micro-adjustments and mechanical wear by holding stable positions and reducing transitions. Its five positions match the five singleton consequents.

### 2.4.8 Servo Offset Calibration

Equation (5) applies the mechanical calibration offset before servo PWM output [12], [28].

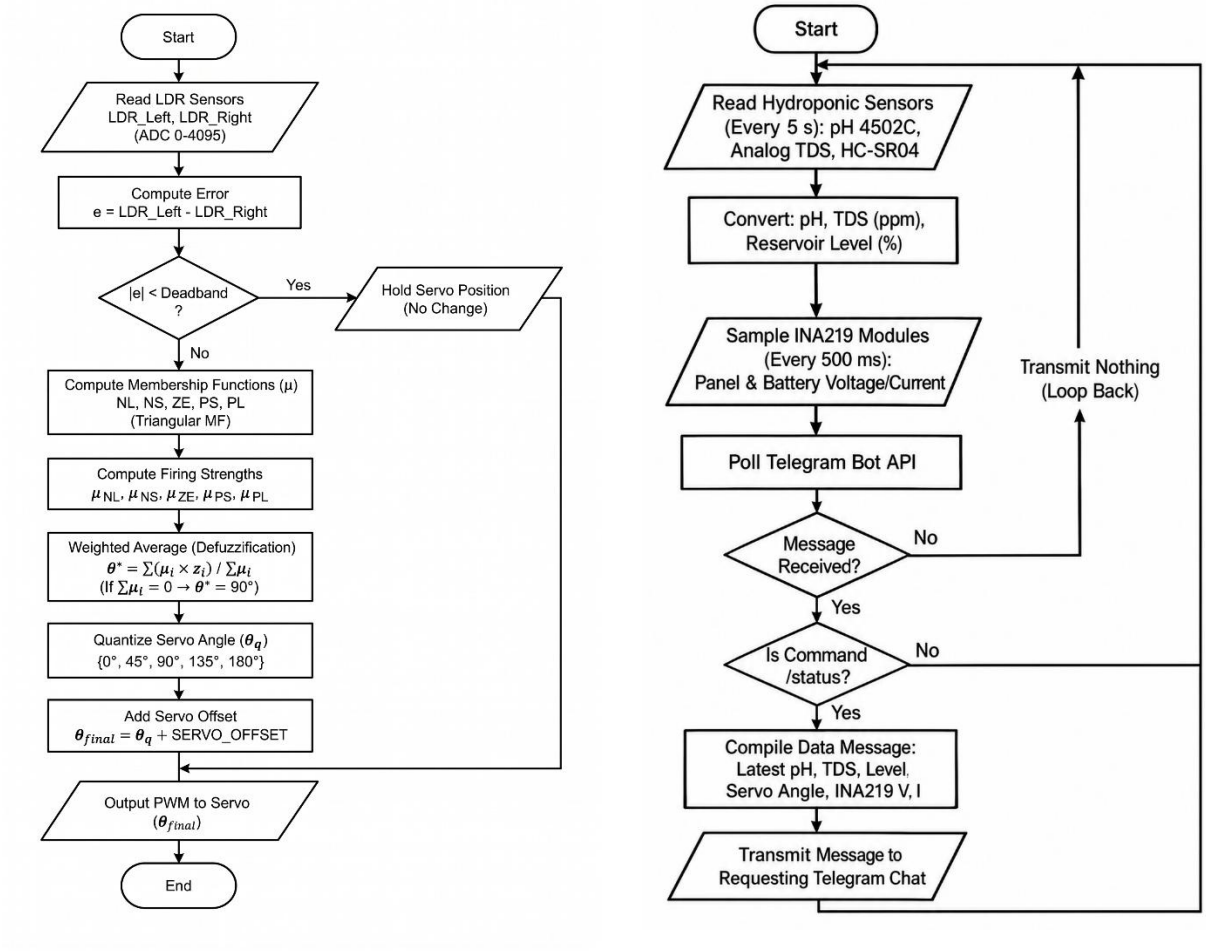
$$Servo_{Final} = \theta_{quantized} + SERVO_{offset} \quad (5)$$

The $SERVO_{offset}$ is an empirically calibrated, signed degree constant stored in firmware. It corrects servo-horn/frame mounting tolerances so commanded angles match physical orientation relative to the horizon. Recalibration is required after mechanical changes.

### 2.4.9 Control Algorithm Flowchart

Figure 7(a)'s ESP32-S3 loop reads LDRs, calculates e (Equation 1), and holds/exits within deadband (Equation 2). Otherwise it computes memberships/rule strengths (Equation 3), weighted θ* (Equation 4, default 90° for Σμ = 0), quantizes (Table 4), adds offset (Equation 5), and outputs PWM.

Figure 7(b) samples pH 4502C, TDS, and HC-SR04 every 5 s into latest unfiltered pH/TDS (ppm)/level (%) values, and INA219 voltage/current every 500 ms (Section 2.4.10). Telegram polling every 8 s transmits nothing without a valid /status request, which returns those latest hydroponic readings, servo angle, and battery voltage/current to the requesting chat. Operator demand determines reporting frequency.




(a) (b)

**Figure 7**. (a) Flowchart of the Zero-Order Fuzzy TSK Solar Tracker Control Algorithm on controller ESP32-S3-Implementation. (b) Flowchart of The Hydroponic Monitoring and on-Demand Telemetry Routine.

### 2.4.10 INA219 Energy Monitoring

INA219 No. 1 (panel-SCC, I²C 0x40) and No. 2 (battery-load, I²C 0x41) sample voltage/current every 500 ms [7]. Equation (6)'s $P_{Panel}(t)$ is trapezoidally integrated over 07:00–17:00 WIB [8], [9]. $E_{tracker}$ and $E_{Fixed}$ are cumulative daily tracking and fixed-panel yields (Wh), respectively, under comparable irradiance.

$$P_{Panel(t)} = V_{OC(t)}\ x\ I_{SC(t)}\ [W] \quad (6)$$

Equation (7) calculates relative energy gain ηgain (%), consistent with [10], [33].

$$\eta_{gain} = \frac{E_{tracker} - E_{fixed}}{E_{fixed}} \; x \; 100\% \quad (7)$$

### 2.4.11 Experimental Procedure

Sensor sampling every 5 seconds follows comparable ESP32 nodes [14], retaining records over 15 minutes. Telegram polling every 8 seconds replies only to /status with pH, TDS (ppm), level, servo angle, and battery voltage/current. Continuous Wi-Fi explains Table 6's modem load and follows agricultural monitoring practice [34-35].

Continuous sensing and telemetry must be included in energy sizing. Comparable greenhouse ESP32 nodes report 8.91 Wh/day [16], with similar consumption in residential PV monitoring using current-voltage sensing [18]. Section 2.5 quantifies this platform's load.

Five consecutive days were tested at Banjarsari (07:00–17:00 WIB), comparing a fixed baseline (servo at 90°) with full TSK tracking. Table 5 classifies Clear, Partially Cloudy, and Overcast conditions from INA219 peak power and daily yield, following quantitative PV sky classification [42-43] and Ponce-Jara et al.'s weather stratification [10]. The phases ran on adjacent days under comparable weather to reduce irradiance confounding [8-9].

**Table 5.** Weather Classification Thresholds

| Category | Peak Power | E_tracker Daily Yield |
|---|---|---|
| Clear | ≥ 30.0 W | ≥ 250.0 Wh |
| Partially Cloudy | 20.0 W ≤ P_peak < 30.0 W | 200.0Wh ≤ E_daily < 250.0 Wh |
| Overcast | < 20.0 W | < 200.0 Wh |

## 2.5 Power Consumption Components and Servo Mechanical Analysis

Table 6 profiles the platform load for autonomy assessment [15], [18]. Continuous ESP32-S3, sensor, and Wi-Fi demand totals 3.85 W or 92.4 Wh/day, above a comparable node's 8.91 Wh/day [16] because of continuously excited analog probes and repeated ultrasonic pulses. Including servo actuation and the tabulated overhead, total demand is 115.88 Wh/day, below the reported 243.78 Wh mean harvest (Section 3).

**Table 6.** System Energy Consumption Profile

| Component | Operational Voltage | Active Current | Power | Daily Operation | Daily Energy |
|---|---|---|---|---|---|
| ESP32-S3 MCU | 5.0 V | 160 mA | 0.80 W | 24 hours | 19.20 Wh |
| Sensors (pH, TDS, HC-SR04) | 5.0 V | 50 mA | 0.25 W | 24 hours | 6.00 Wh |
| Wi-Fi Modem Node | 5.0 V | 560 mA | 2.80 W | 24 hours | 67.20 Wh |
| TD8120MG Servo (Actuation) | 5.0 V | 800 mA (stall 2.5 A) | 4.00 W | ≈0.17 h/day (10 steps) | 0.68 Wh |
| System Baseline Overhead | 12.0 V | 190 mA | 2.28 W | 10 hours | 22.80 Wh |
| Total Estimated | - | - | - | - | 115.88 Wh/day |

Azimuth rotation about the vertical mast (Figure 4) means panel weight creates no driving torque about that axis, although it loads the support and affects friction. Servo demand arises primarily from bearing/gearbox friction and aerodynamic drag, governed by frontal area, drag coefficient, and air speed [44].

The flexible 100 Wp panel weighs below 5 kg. The flat-plate model assumes A ≈ 0.65 m² and Cd ≈ 1.2, consistent with near-perpendicular PV wind-load measurements [45]. Area is estimated from nominal module dimensions and requires actual measurement for final design. Assumed v = 1.0 m/s represents sheltered greenhouse airflow, not extreme outdoor wind. This is an operating-load estimate rather than a site-specific extreme-wind design [46]. Equation (8) gives approximately 0.47 N drag.

$$F = \frac{1}{2}\,\rho C_d A v^2 \;\approx 0.47N \tag{8}$$

Acting at a moment arm of $d \approx 0.3$ m from the mast axis to the panel's center of pressure, corresponding approximately to half the panel width, the resulting wind-induced torque is estimated using Equation (9). The calculated torque is approximately 14 N or 1.4 kg.

$$\tau_{\text{wind}} = \text{F} \times \text{d} \;\approx 0.4\,\text{N}\cdot\text{m} \;\approx 1.4\,kg\cdot cm \tag{9}$$

Against manufacturer stall torque of 15–20 kg (up to 22.8 kg at higher voltage), the lower 15 kg rating gives $Sf = 15/1.4 \approx 10.7$. This supports a static margin for the assumed aerodynamic load only. Estimated parameters do not establish site-specific wind-load safety.

## 3. Results and Discussion

### 3.1 Solar Tracker Dynamic Response and Servo Positioning Analysis

Figure 8's Day 1 trajectory follows {0°, 45°, 90°, 135°, 180°}, matching Thungsuk et al.'s [8] low-latitude discrete tracking. The 90° hold around 09:30–14:10 WIB reflects ZE (|e| < 300 ADC) dominance near alignment [30-31]. Absence of hunting supports quantization's stabilizing function [38].

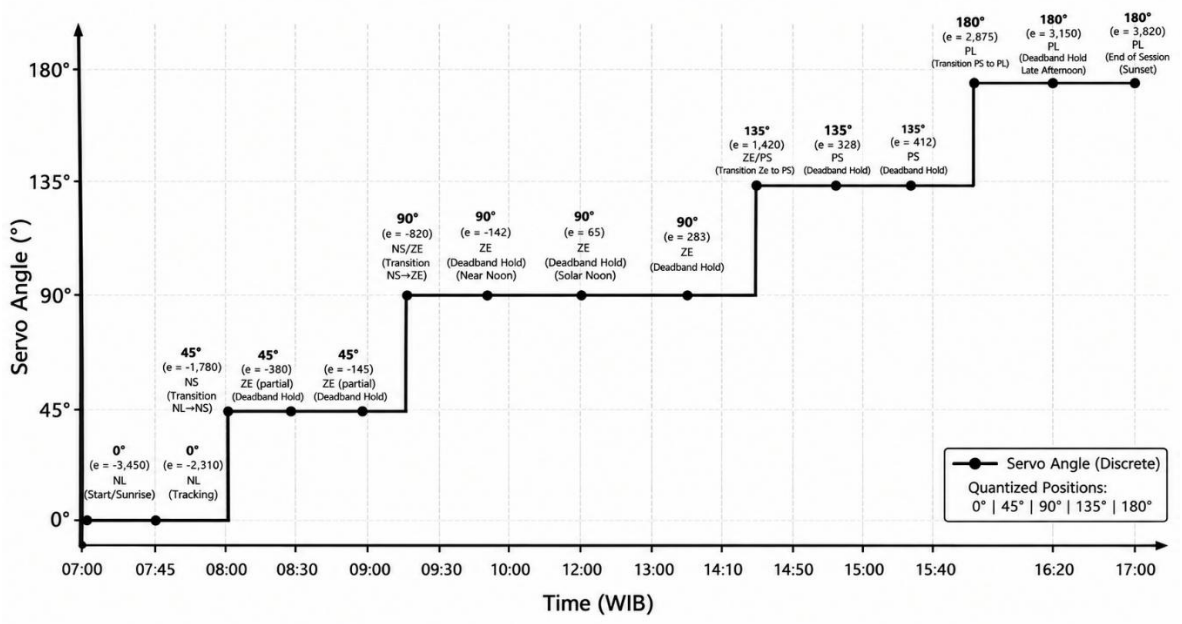



**Figure 8.** Servo Motor Discrete Angular Position over a Representative Test Day (07:00-17:00 WIB).

### 3.2 Fuzzy TSK Membership Function and Rule Activation Analysis

Table 7 traces Day 1 errors, fuzzy activation, and servo positions against expected TSK behavior [1], [21]. At 07:00–08:00 WIB, errors of −3450 to −1780 ADC activate NL then NS, moving from 0° to 45° as the sun moves eastward [36]. Decreasing error shifts NL to NS as alignment improves [24].

**Table 7.** Servo Position Trajectory Representative Clear Day (Day 1, 07:00–17:00 WIB)

| Time (WIB) | e (ADC) | Servo Angle | Active Fuzzy Set | Status |
|---|---|---|---|---|
| 07:00 | −3,450 | 0° | NL | Start (Sunrise) |
| 07:45 | −2,310 | 0° | NL | Tracking (NL Active) |
| 08:00 | −1,780 | 45° | NS | Transition NL→NS |
| 08:30 | −380 | 45° | ZE (partial) | Deadband Hold |
| 09:00 | −145 | 45° | ZE (partial) | Deadband Hold |
| 09:30 | −820 | 90° | NS/ZE | Transition NS→ZE |
| 10:00 | −142 | 90° | ZE | Deadband Hold (Near Noon) |
| 12:00 | 65 | 90° | ZE | Deadband Hold (Solar Noon) |
| 13:00 | 283 | 90° | ZE | Deadband Hold |
| 14:10 | 1,420 | 90° to 135° | ZE/PS | Transition Ze to PS |
| 14:50 | 328 | 135° | PS | Deadband Hold |
| 15:00 | 412 | 135° | PS | Deadband Hold |
| 15:40 | 2,875 | 135° to 180° | PL | Transition PS to PL |
| 16:20 | 3,150 | 180° | PL | Deadband Hold (Late Afternoon) |
| 17:00 | 3,820 | 180° | PL | End of Session (Sunset) |

Near-zero error between 08:30 and 14:10 WIB favors ZE [5], with the servo mainly at 90°. Holds occur at 08:30, 09:00, 10:00, 12:00, and 13:00 WIB, longest near noon as $\mu_{ZE}$ approaches unity, suppressing unnecessary movement while preserving alignment [39].

Increasing afternoon positive errors shift ZE to PS and PL [23], moving 90° to 135° at 14:10 WIB and 180° at 15:40 WIB (Table 7). The NL–NS–ZE–PS–PL sequence at 7.56°S resembles Rahman et al.'s LDR progression [31]. Five singleton rules provide practical angular resolution without Mamdani defuzzification overhead [22], supporting real-time ESP32-S3 control.

**Table 8.** Five Day Summary of Trials

| Day | Weather Condition | Mean \|e\| (ADC) | Deadband Rate (%) | Transitions/hour | Tracking Coverage (%) |
|---|---|---|---|---|---|
| Day 1 | Clear | 138 | 62.3% | 0.5 | 83.7% |
| Day 2 | Part. Cloudy | 187 | 51.4% | 1.2 | 77.2% |
| Day 3 | Part. Cloudy | 162 | 55.7% | 0.9 | 79.6% |
| Day 4 | Clear | 124 | 65.1% | 0.4 | 85.4% |
| Day 5 | Overcast | 246 | 41.8% | 1.8 | 68.3% |
| Mean | All Days | 171 | 55.3% | 1.0 | 78.8% |

Table 8 contrasts clear Days 1/4 (124–138 ADC error, 62.3–65.1% deadband, 0.4–0.5 transitions/hour) with overcast Day 5 (246 ADC, 41.8%, 1.8/hour). Diffuse fluctuating light increases corrections, but five-position quantization restrains hunting. Mean coverage of 78.8% compares with Thungsuk et al.'s 75.0–85.0% equatorial LDR range [8].

The 55.3% mean hold rate represents 5.53 of 10 daily measurement hours without actuation. At 1.0 transition/hour, approximately 10 daily position changes reduce actuator cycling and support TD8120MG longevity in humid greenhouses.

### 3.3 Power Monitoring and Energy Efficiency Analysis

Table 9 reports five-day INA219 yields. Figure 9's clear Day 1 power profiles favor near-optimal discrete TSK positioning over the fixed panel, especially during peak irradiance at 10:00–14:00 WIB.

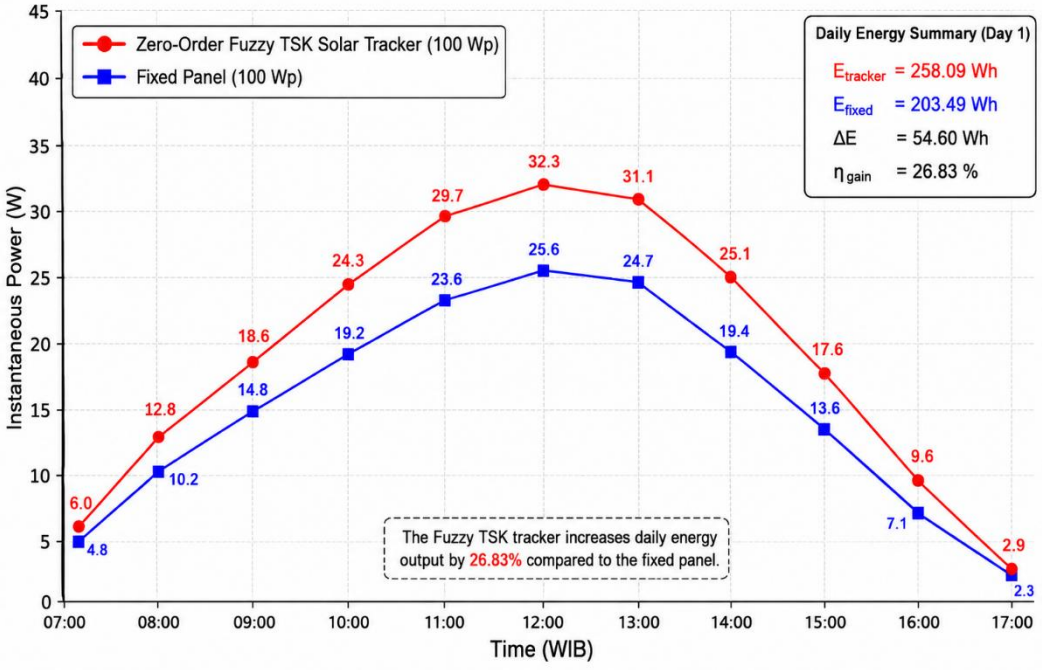



**Figure 9.** Comparative Instantaneous Panel Power Output: Fixed Panel 100Wp vs. Zero-Order Fuzzy TSK Solar Tracker Panel 100WP.

**Table 9.** Solar Tracker Dynamic Performance Five Day Summary (Banjarsari Site, 07:00 - 17:00)

| Date | E_fixed (Wh) | E_tracker (Wh) | ΔE (Wh) | η_gain (%) |
|---|---|---|---|---|
| Day 1 | 203.49 | 258.09 | 54.60 | 26.83 |
| Day 2 | 191.34 | 245.87 | 54.53 | 28.50 |
| Day 3 | 198.72 | 251.44 | 52.72 | 26.53 |
| Day 4 | 207.18 | 266.93 | 59.75 | 28.84 |
| Day 5 | 165.41 | 196.55 | 31.14 | 18.83 |
| Average | 193.23 | 243.78 | 50.55 | 25.91 |

Mean daily yield was 243.78 Wh versus 193.23 Wh fixed, with 25.91% mean daily gain over five days. A paired *t*-test of the five matched $E_{fixed}/E_{tracker}$ pairs in Table 9 showed a tracker advantage ($t(4) = 10.13$, $p < 0.001$, Cohen's $d = 4.53$, 95% CI for mean gain [36.7, 64.4] Wh). With n = 5 days, this within-study effect requires longer independent replication before population generalization.

The 25.91% *gross* gain excludes ≈0.68 Wh/day servo energy for ≈10 repositionings (Table 6). Common ESP32-S3, sensor, and Wi-Fi loads cancel in the *net* comparison. Subtracting servo energy from each daily ΔE gives 25.55% *net* gain, 0.36 percentage points lower. Parasitic actuation therefore does not negate the harvesting benefit.

Table 10 gives gains of 27.84% (Clear), 27.52% (Partially Cloudy), and 18.83% (Overcast, Day 5). Diffuse light reduces differential LDR irradiance and correctable pointing error. The 25.91% average is weather-dependent, reflecting the specific 3 Clear/Partly-Cloudy 1 Overcast day ratio observed. A full rainy-to-dry seasonal deployment is needed for a representative mean.

**Table 10.** Performance Gains of the Solar Tracking System under Different Weather Conditions

| Weather Category | Days | Gross Gain (%) | Mean Gross Gain (%) | Net Gain (%) |
|---|---|---|---|---|
| Clear | 1 and 4 | 26.83, 28.84 | 27.84 | ≈27.5 |
| Partially Cloudy | 2 and 3 | 28.50, 26.53 | 27.52 | ≈27.2 |
| Overcast | 5 | 18.83 | 18.83 | ≈18.4 |
| All days (weighted) | 1–5 | | 25.91 (simple mean) / 26.16 (energy-weighted) | 25.55 |

Energy-weighted gain ($\Sigma\Delta E / \Sigma E_{fixed} = 26.16\%$) exceeds the 25.91% simple daily mean because the low-baseline overcast Day 5 receives less weight when energy is pooled.

### 3.4 Energy Efficiency Analysis and Literature Comparison

Table 9's gains fit the tropical/equatorial single-axis benchmark of 20–40% [2], [5]. Ponce-Jara et al. [10] achieved up to 37.0% at 0.0°S. Thungsuk et al. [8] reported 23.3% with five-position tracking. Proportional TSK weighted averaging [27] smooths transitions relative to binary stepping, yielding 25.91% gross and 25.55% net. Table 11 compares Hariri et al.'s PID LDR tracker without fuzzy reasoning [28] and Sanyal et al.'s on–off/fuzzy study without quantitative energy accounting [30]. To the authors' knowledge, this is the first hardware-validated combination of Zero-Order TSK, deadband, and INA219 energy monitoring on a self-powered IoT hydroponic platform.

**Table 11.** Comparative Analysis of Solar Tracking Systems

| Reference (Year) | Control Method | Tracker Type | Energy Gain (%) | Key Contribution |
|---|---|---|---|---|
| Saeedi [11] (2021) | Wheatstone Bridge Threshold | Dual-axis | N/R | High-precision LDR sensing without intelligent control. |
| Hariri [28] (2022) | LDR Sensor-based PID | Single-axis | 7.70 | Experimental LDR-based versus azimuth-based control; no fuzzy reasoning or deadband. |
| Boukdir [12] (2022) | Three-LDR Threshold | Dual-axis | N/R | Improved positioning using three sensors; no fuzzy reasoning. |
| Thungsuk [8] (2023) | Open-loop five-positions | Single-axis | 23.30 | Five-position tracker without fuzzy control or IoT. |
| Demirdelen [9] (2023) | Astronomical Timer | Various | 30–35 | GPS/timer scheduling without LDR feedback. |
| Ponce-Jara [10] (2024) | Continuous LDR Threshold | Single-axis | 37.00 | High energy gain using continuous tracking; no fuzzy TSK. |
| Rahman [31] (2024) | Mamdani Fuzzy + LDR | Dual-axis | N/R | ESP32-based fuzzy LDR tracking; no deadband and no singleton TSK inference. |
| Sanyal [30] (2024) | On–off versus Fuzzy Logic | Dual-axis | N/R | Low-cost hardware prototype; no quantitative energy accounting. |
| Hammas [32] (2025) | Hybrid LDR + GPS | Dual-axis | ≈30 | Hybrid positioning with higher mechanical complexity. |
| This Study (2026) | Zero-Order Fuzzy TSK + Deadband | Single-axis | 25.91 | 25.91 gain energy average using Takagi Sugeno Kang Fuzzy Logic and Deadband combined with IOT monitoring. |

### 3.5 The Intelligent Characteristics of the Zero-Order Fuzzy TSK Tracker

"Intelligent" denotes TSK rule-based interpretation of LDR error [23], [31], generating proportional actions from expert rules rather than threshold-only switching. First, five IF-THEN rules encode solar-trajectory knowledge. Second, Zero-Order TSK weighted averaging generates proportional output [22], [27].

$$\theta * = \Sigma(\mu i \times zi) \,/\, \Sigma \mu i \tag{10}$$

Third, overlapping triangles [36] assign errors to multiple linguistic categories, smoothing transitions under uncertainty. Fourth, deadband decisions [38], [39] permit movement only when $|e| \geq \mathrm{LD}R_{deadband}$ and hold the actuator when $|e| < \mathrm{LD}R_{deadband}$.

Rule-based reasoning, proportional output, overlapping-set uncertainty handling, and autonomous hold decisions distinguish the system from threshold trackers [28], [30] and earlier Mamdani implementations [21], [37].

### 3.6 Economic and Cost-Benefit Analysis

Table 12 compares the tracked 100 Wp system with a hypothetical static 150 Wp installation. Static systems avoid tracking mechanics but require oversizing to offset diurnal cosine losses and sustain always-on IoT loads [9].

The ESP32-S3 already serves hydroponic telemetry. Tracking therefore adds only the servo, dual LDRs, and mounting, estimated at $15–$20. A 100-to-150 Wp panel upgrade costs more and occupies additional greenhouse space [1].

**Table 12.** Cost Comparison: Tracked 100Wp vs Static 150Wp

| Component / Parameter | Tracked 100 Wp | Static 150 Wp |
|---|---|---|
| Solar Panel Monocrystaline | ~$16.38 (100 Wp) | ~$49.71 (150 Wp) |
| Microcontroller (ESP32-S3) | $4.52 (Shared IoT baseline) | $0.00 (Shared IoT baseline) |
| Tracking Actuator & Sensors | ~$8.93 (Servo + 2x LDR) | $0.00 |
| Mechanical Mounting | ~$12.00 (Rotational axis) | ~$14.00 (Fixed frame) |
| Total Estimated Cost | ~$41.83 | ~$63.71 |
| Daily Power Profile | Extended charging window [10] | Peaked around solar at noon |
| Battery Service Life | Extended (Lower Depth of Discharge) | Standard (Higher peak load) |
| Physical Footprint | ≈ 0.65 m² (Space-efficient) | ≈ 0.95 m² (Larger dimension) |

Tracking broadens the power curve, extending charging into early morning and late afternoon [8]. This reduces daily battery depth of discharge (DoD). Because lifespan is inversely related to DoD, the longer service life lowers replacement and operational costs (OPEX). Together with competitive capital expenditure and reduced footprint, this supports the lifecycle cost-benefit argument for using the existing ESP32-S3 with a tracker rather than purchasing a larger static panel.

### 3.7 Operational Performance of the Hydroponic Water Quality Monitoring

Table 13 contains four combined tracker/water-quality Telegram replies from 15–19 August 2026, including pH 8.48/TDS 520 ppm after noon on 15 August and pH 6.96/TDS 376 ppm on 19 August.

**Table 13.** Representative On-Demand Telegram Responses

| Date / Time | pH (status) | TDS, ppm (status) | Servo (°) | Battery, V (cal.) | Current, A (cal.) | Tank level (status) |
|---|---|---|---|---|---|---|
| 15 Aug, 12:41 | 8.48 (High Alkaline pH) | 520 (GOOD) | 45° | 12.151V | 0.188A | 30% (Normal) |
| 15 Aug, 18:54 | 8.00 (Slightly Alkaline pH) | 124 (BAD) | 90° | 12.111V | 0.124A | 31% (Normal) |
| 16 Aug, 09:44 | 7.78 (Slightly Alkaline pH) | 661 (GOOD) | 45° | 12.031V | 0.134A | 27% (Normal) |
| 19 Aug, 11:08 | 6.96 (Ideal) | 376 (BAD) | 45° | 11.985V | 0.187A | 30% (Normal) |

Variable pH (6.96–8.48) and TDS (124–661 ppm) indicate responsive probes and a managed reservoir. pH shifts from High Alkaline on 15 August toward Ideal on 19 August. TDS alternates between firmware GOOD/BAD categories. HC-SR04 detects 27% on 16 August within the stated Normal range (25–31%). Battery voltage remains operational at 11.985–12.151 V across all four snapshots, without approaching critical deep discharge. Four successful replies demonstrate combined on-demand telemetry and responsive sensors. These irregular instantaneous, unfiltered snapshots do not provide continuous logging, a delivery-success rate, an overnight battery-discharge profile, or suppression of short-term noise.

## 4. Conclusion

The ESP32-S3 Zero-Order TSK melon hydroponic platform combines differential LDR input, five triangular sets, and deadband control without Mamdani centroid integration. Five-day Jombang trials with dual INA219s yielded 243.78 Wh/day versus 193.23 Wh/day fixed, corresponding to 25.91% gross and 25.55% net gain. The actuator held for 55.3% of the window with roughly 1.0 transition/hour. Four Telegram snapshots returned tracker state, pH, TDS, and water level, demonstrating a functioning self-powered greenhouse IoT node.

The hobby-grade TD8120MG limits panels to 100 Wp, while quantized single-axis control leaves pointing errors. Industrial actuators or slew drives could support larger panels and continuous dual-axis tracking with seasonal compensation. Missing Maximum Power Point Tracking (MPPT) and a static rule base limit recovery and adaptability. Future work should combine INA219-driven MPPT with adaptive TSK/neuro-fuzzy tuning. Multi-month trials across rainy and dry seasons, fixed-interval logging, median/moving-average pH/TDS filtering, and closed-loop nutrient dosing are recommended.

## References

[1] Sadeghi, R., Parenti, M., Memme, S., Fossa, M., & Morchio, S. (2025). A review and comparative analysis of solar tracking systems. *Energies*, *18*(10), 2553.

[2] Paliyal, P. S., Mondal, S., Layek, S., Kuchhal, P., & Pandey, J. K. (2024). Automatic solar tracking system: A review pertaining to advancements and challenges in the current scenario. *Clean Energy*, *8*(6), 237-262.

[3] Ahmad, U., Alvino, A., & Marino, S. (2022). Solar fertigation: A sustainable and smart IoT-based irrigation and fertilization system for efficient water and nutrient management. *Agronomy*, *12*(5), 1012.

[4] Kanwal, T., Rehman, S. U., Ali, T., Mahmood, K., Villar, S. G., Lopez, L. A. D., & Ashraf, I. (2023). An intelligent dual-axis solar tracking system for remote weather monitoring in the agricultural field. *Agriculture*, *13*(8), 1600.

[5] Musa, A., Alozie, E., Suleiman, S. A., Ojo, J. A., & Imoize, A. L. (2023). A review of time-based solar photovoltaic tracking systems. *Information*, *14*(4), 211.

[6] Thilakarathne, N. N., Bakar, M. S. A., Abas, P. E., & Yassin, H. (2025). Internet of things enabled smart agriculture: Current status, latest advancements, challenges and countermeasures. *Heliyon*, *11*(3).

[7] Ullah, S., Hafeez, G., Rukh, G., Albogamy, F. R., Murawwat, S., Ali, F., ... & Rehman, K. (2022). A Smart Sensors-Based Solar-Powered System to Monitor and Control Tube Well for Agriculture Applications. *Processes*, *10*(8), 1654.

[8] Thungsuk, N., Tanaram, T., Chaithanakulwat, A., Savangboon, T., Songruk, A., Mungkung, N., ... & Yuji, T. (2023). Performance analysis of solar tracking systems by five-position angles with a single axis and dual axis. *Energies*, *16*(16), 5869.

[9] Demirdelen, T., Alıcı, H., Esenboğa, B., & Güldürek, M. (2023). Performance and economic analysis of designed different solar tracking systems for Mediterranean climate. *Energies*, *16*(10), 4197.
[10] Ponce-Jara, M. A., Pazmino, I., Moreira-Espinoza, Á., Gunsha-Morales, A., & Rus-Casas, C. (2024). Assessment of single-axis solar tracking system efficiency in equatorial regions: A case study of Manta, Ecuador. *Energies*, *17*(16), 3946.
[11] Saeedi, M., & Effatnejad, R. (2021). A new design of dual-axis solar tracking system with LDR sensors by using the wheatstone bridge circuit. *IEEE sensors journal*, *21*(13), 14915-14922.
[12] Boukdir, Y., & Omari, H. E. (2022). Novel high precision low-cost dual axis sun tracker based on three light sensors. *Heliyon*, *8*(12).
[13] Ghassoul, M. (2021). A dual solar tracking system based on a light to frequency converter using a microcontroller. *Fuel Communications*, *6*, 100007.
[14] Sneineh, A. A., & Shabaneh, A. A. (2023). Design of a smart hydroponics monitoring system using an ESP32 microcontroller and the Internet of Things. *MethodsX*, *11*, 102401.
[15] Hercog, D., Lerher, T., Truntič, M., & Težak, O. (2023). Design and implementation of ESP32-based IoT devices. *Sensors*, *23*(15), 6739.
[16] Saxena, A., Agarwal, A., Nagrath, B., Jayavanth, C. S., Thulasidoss, S., Maheswari, S., & Sasikumar, P. (2025). Deep learning-driven IoT solution for smart tomato farming. *Scientific Reports*, *15*(1), 31092.
[17] Wijayakusuma, P., Hakim, G. P. N., & Li, B. (2025). TerraGrow: Integrated platform for real time plant monitoring and automated watering system with IoT and fuzzy Sugeno Algorithm. *HardwareX*, e00724.
[18] Tradacete-Ágreda, M., Sánchez-Pérez, A., Santos-Pérez, C., Hueros-Barrios, P. J., Rodríguez-Sánchez, F. J., & Espolio-Maestro, J. (2025). Smart energy management for residential PV microgrids: ESP32-based indirect control of commercial inverters for enhanced flexibility. *Sensors*, *25*(21), 6595.
[19] Tang, H. H., & Ahmad, N. S. (2024). Fuzzy logic approach for controlling uncertain and nonlinear systems: a comprehensive review of applications and advances. *Systems Science & Control Engineering*, *12*(1), 2394429.
[20] Yesil, B., & Sahin, S. (2025). Real-time implementation of a microcontroller-based coupled-tank water level control system with feedback linearization and fuzzy logic controller algorithms. *Sensors*, *25*(5), 1279.
[21] Vidal-Martínez, R., García-Martínez, J. R., Rojas-Galván, R., Álvarez-Alvarado, J. M., González-Lee, M., & Rodríguez-Reséndiz, J. (2025). A review of Mamdani, Takagi–Sugeno, and Type-2 fuzzy controllers for MPPT and power management in photovoltaic systems. *Technologies*, *13*(9), 422.
[22] Samavat, T., Nazari, M., Ghalehnoie, M., Nasab, M. A., Zand, M., Sanjeevikumar, P., & Khan, B. (2023). A comparative Analysis of the Mamdani and Sugeno Fuzzy Inference systems for MPPT of an ISlanded PV System. *International Journal of Energy Research*, *2023*(1), 7676113.
[23] Maqekeni, S., Obileke, K., Ndiweni, O., & Mukumba, P. (2025). Application of fuzzy logic techniques in solar energy systems: a review. *Applied System Innovation*, *8*(5), 144.
[24] Hadroug, N., Iratni, A., Hafaifa, A., Boudjemline, A., Alshammari, O. S., Jerbi, H., ... & Chen, X. (2023). Energy efficiency improvement in photovoltaic installation using a twin-axis solar tracking mechanism with LDR sensors compared with neuro-fuzzy adaptive inference structure. *Journal of Electrical Engineering & Technology*, *18*(4), 2943-2967.
[25] Teso-Fz-Betoño, D., Aramendia, I., Ramos-Hernanz, J. A., Portal-Porras, K., Caballero-Martin, D., & Lopez-Guede, J. M. (2026). Real-Time Edge Deployment of ANFIS for IoT Energy Optimization. *Processes*, *14*(6), 1004.

[26] Martínez-González, A., Moreno-Hernández, D., Zamarripa-Ramírez, J. C. I., & Ortega-Martínez, O. F. (2025). Design and Implementation of a Fuzzy Logic Algorithm Embedded in a Microcontroller for Combustion Applications: A. Martínez-González et al. *International Journal of Fuzzy Systems*, 1-16.

[27] Zhang, Y., Wang, G., Zhou, T., Huang, X., Lam, S., Sheng, J., ... & Ding, W. (2024). Takagi-Sugeno-Kang fuzzy system fusion: A survey at hierarchical, wide and stacked levels. *Information fusion*, *101*, 101977.

[28] Hariri, N. G., AlMutawa, M. A., Osman, I. S., AlMadani, I. K., Almahdi, A. M., & Ali, S. (2022). Experimental investigation of azimuth-and sensor-based control strategies for a PV solar tracking application. *Applied Sciences*, *12*(9), 4758.

[29] Chenchireddy, K., Gouse Basha Mulla, V. J., Sultana, W., Sydu, S. A., & Giddalur, E. (2025). Solar tracker using Arduino microcontroller and light dependent resistor. *International Journal of Power Electronics and Drive Systems (IJPEDS)*, *16*(1), 70-75.

[30] Sanyal, A., Mohanta, J. C., & Faiyaz Ahmed, M. D. (2026). Development of a dual-axis solar tracker for efficient sun energy harvesting. *Proceedings of the Institution of Mechanical Engineers, Part E: Journal of Process Mechanical Engineering*, *240*(1), 888-900.

[31] Rahman, A. F. S., Fattah, A., Asni, A., Waruni, M., Kasrani, & Ardiansyah, W. (2024, March). Fuzzy logic control system for optimizing dual-axis solar panel tracking. In *E3S Web of Conferences* (Vol. 500, p. 03021). EDP Sciences.

[32] Hammas, M., Fituri, H., Shour, A., Khan, A. A., Khan, U. A., & Ahmed, S. (2025). A hybrid dual-axis solar tracking system: Combining light-sensing and time-based GPS for optimal energy efficiency. *Energies*, *18*(1), 217.

[33] Ismail, F. B., Rahmat, M. A. A., Kazem, H. A., Al-Obaidi, A. S. M., & Ridwan, M. S. (2024). Maximizing energy via solar-powered smart irrigation: An approach utilizing a single-axis solar tracking mechanism. *Irrigation and Drainage*, *73*(3), 829-845.

[34] Tatas, K., Al-Zoubi, A., Christofides, N., Zannettis, C., Chrysostomou, M., Panteli, S., & Antoniou, A. (2022). Reliable IoT-based monitoring and control of hydroponic systems. *Technologies*, *10*(1), 26.

[35] Jaliyagoda, N., Lokuge, S., Gunathilake, P. M. P. C., Amaratunga, K. S. P., Weerakkody, W. A. P., Bandaranayake, P. C., & Bandaranayake, A. U. (2023). Internet of things (IoT) for smart agriculture: Assembling and assessment of a low-cost IoT system for polytunnels. *Plos one*, *18*(5), e0278440.

[36] K. Gatea and A. Dheyab. (2024). Design and Analysis of the Effect of the Number of Membership Functions on the Accuracy of the Fuzzy Controller in a Sun Tracking System, *International Journal of Technology and Systems*, vol. 9, no. 4, pp. 37–47.

[37] Pop, M. D., Pescaru, D., & Micea, M. V. (2023). Mamdani vs. Takagi–Sugeno fuzzy inference systems in the calibration of continuous-time car-following models. *Sensors*, *23*(21), 8791.

[38] Domański, P. D. (2022). Improving actuator wearing using noise filtering. *Sensors*, *22*(22), 8910.

[39] Fortaleza, E. L., Gomes, L. M., Limaverde Filho, J. O. D. A., de Campos, M. C., Longhi, L. G. S., de Lima, M. L., & Tognetti, E. S. (2022). Model-free adaptive filter to mitigate actuator wear. *ISA transactions*, *129*, 493-504.

[40] Mansoor, S., Iqbal, S., Popescu, S. M., Kim, S. L., Chung, Y. S., & Baek, J. H. (2025). Integration of smart sensors and IOT in precision agriculture: trends, challenges and future prospectives. *Frontiers in Plant Science*, *16*, 1587869.

[41] Liu, Y., Liu, Y., Shao, Q., Wang, R., & Lv, Y. (2024). A Novel Neuro-fuzzy Learning Algorithm for First-Order Takagi–Sugeno Fuzzy Model: Caputo Fractional-Order Gradient Descent Method: Y. Liu et al. *International Journal of Fuzzy Systems*, *26*(8), 2616-2631.

[42] Poddar, S., Kay, M., & Boland, J. (2024). A standardized sky condition classification method for multiple timescales and its applications in the solar industry. *Energies*, *17*(18), 4616.
[43] Benavides Cesar, L., & Perpiñán-Lamigueiro, O. (2025). Solar irradiance ramp classification using the IBEDI (Irradiance-based extreme day identification) method. *Energies*, *18*(2), 243.
[44] You, J., Lim, M., You, K., & Lee, C. (2021). Wind coefficient distribution of arranged ground photovoltaic panels. *Sustainability*, *13*(7), 3944.
[45] Yao, J., Tu, Z., Wang, D., Shen, G., & Lou, W. (2022). Experimental investigation of wind loads on roof-mounted solar arrays. *Sustainability*, *14*(14), 8477.
[46] Liang, B., Zhao, S., Li, Y., Wang, P., Liu, Z., Zhang, J., & Ding, T. (2022). Study on the natural ventilation characteristics of a solar greenhouse in a high-altitude area. *Agronomy*, *12*(10), 2387.